ACKNOWLEDGMENT

This work was supported by the UK Engineering and Physical Science Research Council under grant EP/H049606/1.

REFERENCES

1. H.I. Cantu and V. Fusco, Detection sensitivity of self-pulsed self-oscillating millimetre-wave sensor, Electron Lett 43 (2007), 1013–1015.
2. G. Xiaorong, J. Sun, C. Wang, and C. Yuan, CMOS yields UHF RFID transmitter, In: Microwaves and RF, February 2012.
3. S.J. Thomas, E. Wheeler, J. Teizer, and M.S. Reynolds, Quadrature amplitude modulated backscatter in passive and semipassive UHF RFID systems, IEEE Trans Microwave Theory Tech 60 (2012), 1175–1182.
4. R. Adler, A study of locking phenomena in oscillators, Proc IRE 34 (1946), 351–357.
5. K. Kurokawa, Injection locking of microwave solid-state oscillators, Proc IEEE 61 (1973), 1386–1392.

A NOVEL PHOTONIC CRYSTAL BAND-PASS FILTER USING DEGENERATE MODES OF A POINT-DEFECT MICROCAVITY FOR TERAHERTZ COMMUNICATION SYSTEMS

Chen Chun-Ping,[1] Tetsuo Anada,[1] Stephen Greedy,[2] Trevor M. Benson,[2] and Phillip Sewell[2]
[1] Department of Electrical engineering, Kanagawa University, Kanagawa, Japan
[2] Department of Electrical and Electronic Engineering, George Green Institute for Electromagnetics Research, University of Nottingham, Nottingham, NG7 2RD, United Kingdom; Corresponding author: steve.greedy@nottingham.ac.uk

Received 8 November 2013

ABSTRACT: *Compact devices are important for the realization of terahertz communications systems. This article proposes a novel photonic crystal-based device for realizing microminiature, high-selectivity high Q band-pass filters (BPF) and the design of a dual-mode square lattice photonic crystal BPF that utilizes the degenerated modes of a point defect microcavity is presented. To design a high Q microcavity, the photonic band-gap is initially calculated using the plane wave expansion method. Second, the eigenfrequencies and modal fields of a point defect microcavity that generates localized states in the band-gap are calculated by a supercell method. Finally, the characteristics of mode splitting and the proposed dual-mode BPFs are numerically studied by a full-wave time-domain method.* © 2014 Wiley Periodicals, Inc. Microwave Opt Technol Lett 56:792–797, 2014; View this article online at wileyonlinelibrary.com. DOI 10.1002/mop.28204

Key words: *photonic crystal; band-gap; terahertz; degenerate modes; dual-mode filter; microcavity*

1. INTRODUCTION

Devices operating at submillimeter wavelengths, or within the terahertz (THz) region of the electromagnetic spectrum (i.e., 0.1–10 THz), have allowed the development and realization of systems with new capabilities that span many fields of application; imaging, short-range and wideband secure communications, chemical and biological sensing, and material analysis to name but a few. In [1], a system comprised of electronic and photonic technologies has been demonstrated that is capable of relaying high-definition TV. Operating at a data-rate of 10 Gbit/s over a 120-GHz wireless system, this is a prime example of the utilization of submillimeter wave (sub-MMW) technologies. Compact and low-loss electromagnetic devices are key components for building future sub-MMW-integrated circuits operating at THz frequencies. Recently, a parallel plate metal waveguide in [2] has demonstrated excellent performance for guiding THz pulses with little distortion over a distance of the order of a few centimeters. However, there are some drawbacks with this structure; for example, it is not easy to control the propagation of the wave and the beam can only travel in one direction. To realize fundamental devices (e.g., filters, switches, and splitters), an integrated and compact silicon (Si)-based solid state platform for THz signal propagation, guidance, and control would be preferable. Fortunately, Si-based photonic crystals (PhC) are transparent in the THz range and they have shown promise in their ability to control the propagation of electromagnetic waves at these frequencies. However, problems will exist due to the discontinuities at the interfaces between the different circuit elements; therefore, care is needed when choosing and implementing specific computer-based simulation strategies during the design process.

In this article, we propose and simulate a novel PhC dual-mode band-pass filter (BPF), by integrating a high Q microcavity within a Si-based PhC platform. The resonant frequency splitting of a microcavity, which is important for the BPF design, is presented. Although two-dimensional (2D) PhCs lack a band gap in the direction perpendicular to the lattice plane, they offer substantial advantages in terms of compactness, stability, and fabrication, which make them attractive for THz devices [3, 4].

2. PROPERTIES OF THE 2D PHOTONIC CRYSTAL

2.1. Model of 2D Photonic Crystal in Air

In this article, we consider photonic crystals consisting of a 2D array of dielectric rods. These arrays form either a square or triangular lattice embedded within a parallel-plate metal waveguide. Figure 1 illustrates the case for a square lattice. A waveguide can then be created by introducing a line-defect within the crystal, this defect being surrounded by a finite number of rows, N, of periodically spaced dielectric rods. It is well known that the wave guided by this 2D PhC structure can be decomposed into transverse electric (TE: Ex, Ey, Hz) and transverse magnetic (TM: Hx, Hy, Ez) polarized modes which can also be designated as H-polarized and E-polarized modes, respectively. Various numerical methods have been employed to analyze the band structures and the transmission characteristics for PhC devices, and Figure 2 shows the computed values of the band gaps obtained by using the plane wave expansion method, [5]. To obtain accurate results, with an error of less than 1%, a significant number of component waves is required; 271 were used for those results shown in Figure 2. The band structure is dependent on the geometric and material parameters of the PhC, namely, the lattice parameters defined by the radius (r) and spacing of the rods (a), the refractive indices of the materials and corresponding refractive index contrast. A typical PhC material has a refractive index of $n = 3.4$ (relative dielectric constant of $\varepsilon_r = 11.56$) which, at THz frequencies, corresponds to high-resistivity, high-purity silicon. With lattice parameters of $r/a = 0.175$, where $a = 58.5$ μm and $r = 10.2375$ μm, the PhC has a wide band-gap, for the Ez (TM) polarization in the frequency range of $a/\lambda = 0.31$–0.44, as illustrated in Figure 2 where $\lambda = \omega/2\pi c$, with c being the speed of light in a vacuum.

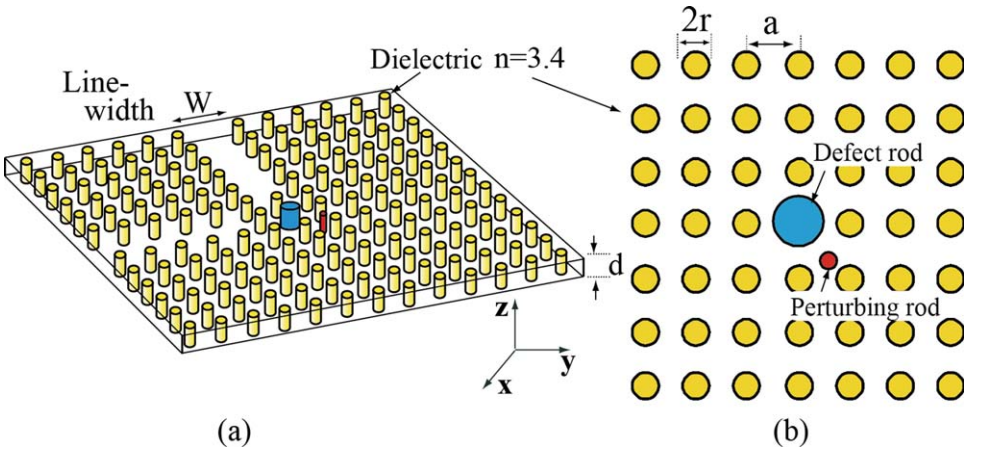

Figure 1 Two-dimensional photonic crystal (PhC) comprised of a square lattice of columns in air that are homogenous along the *z*-axis and periodic along the x- and *y*-directions. (a) Two-dimensional array of dielectric rods in air and (b) 2D 7 × 7 supercell. [Color figure can be viewed in the online issue, which is available at wileyonlinelibrary.com]

There is no corresponding band-gap for the Hz (TE) polarization.

2.2. *Properties of PhC Straight Line Defect Waveguide*

To obtain the transmission characteristics of PhC line-defect waveguides, a time-domain simulation was performed CST's Microwave Studio [6]. The PhC was constructed on a mesh size of $N_x = 919$ by $N_y = 219$ with perfectly matched layers (PML) at the boundaries of the computational window. The line defect was created by removing one row of dielectric rods, as illustrated in Figure 3(a), [7, 8]. The waveguide was excited with a TM Gaussian modulated pulse with a center frequency of 0.35 a/λ. A key factor in designing a PhC waveguide is the propagation loss, $S_{21,}$ which is related to the confinement of the guided mode. Therefore, to validate our approach, simulations were initially performed on these straight waveguides and the convergence of transmission loss as a function of the number of rows, *N*, used to represent the PhC lattice was examined [Fig. 3(a)]. We then obtained the transmission and reflection spectra for the 2D photonic crystal with three rows of dielectric rods, as shown in Figure 3(b). As can be seen from Figure 3(c), the waveguide

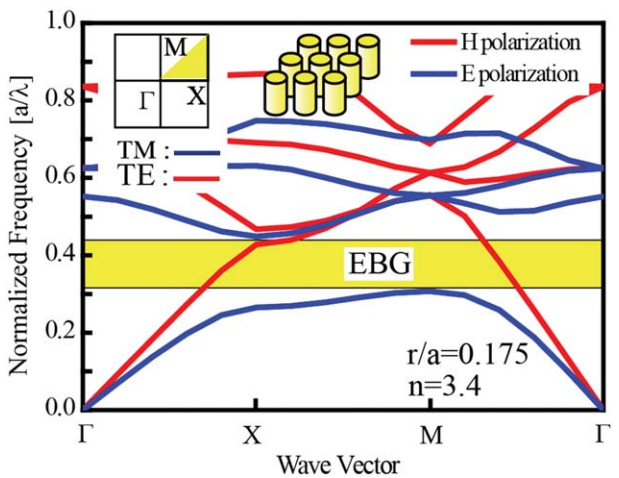

Figure 2 Band structure of a photonic crystal comprised of a square lattice of silicon rods in air calculated using a plane wave expansion method with 271 plane waves. $r/a = 0.175$. [Color figure can be viewed in the online issue, which is available at wileyonlinelibrary.com]

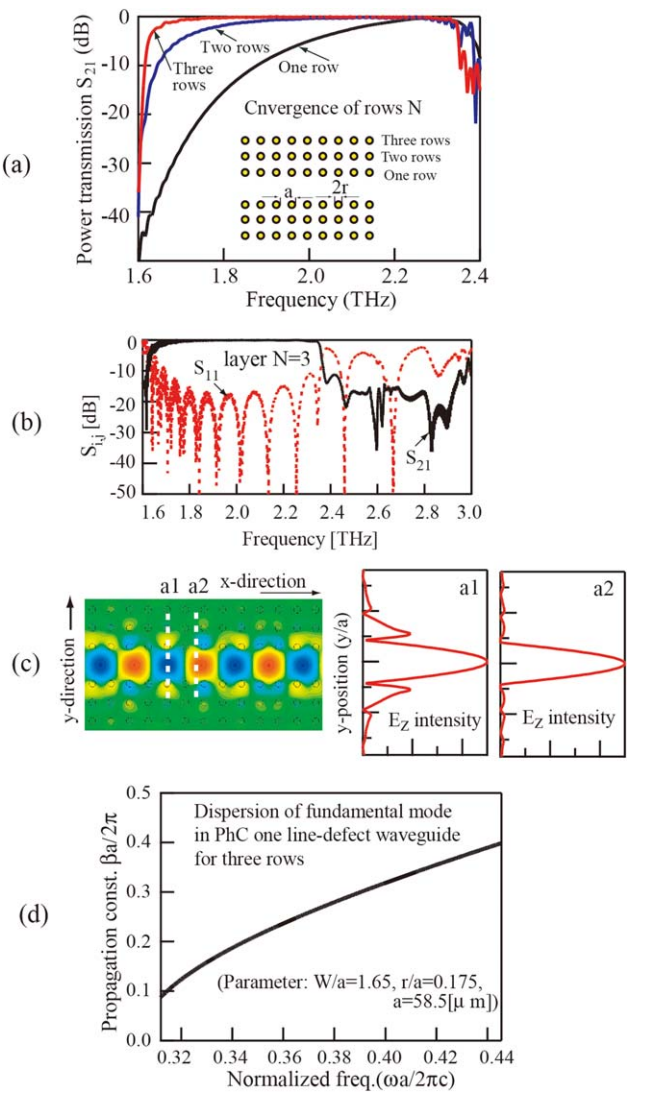

Figure 3 Properties of a straight line in a photonic crystal single defect waveguide. (a) Frequency dependence of power transmission (S_{21}) for 1, 2, and 3 rows, (b) transmission (S_{21}, black) and reflection (S_{11}, red) coefficients for 3 rows, (c) Ez field distribution, (d) dispersion of dominant mode. [Color figure can be viewed in the online issue, which is available at wileyonlinelibrary.com]

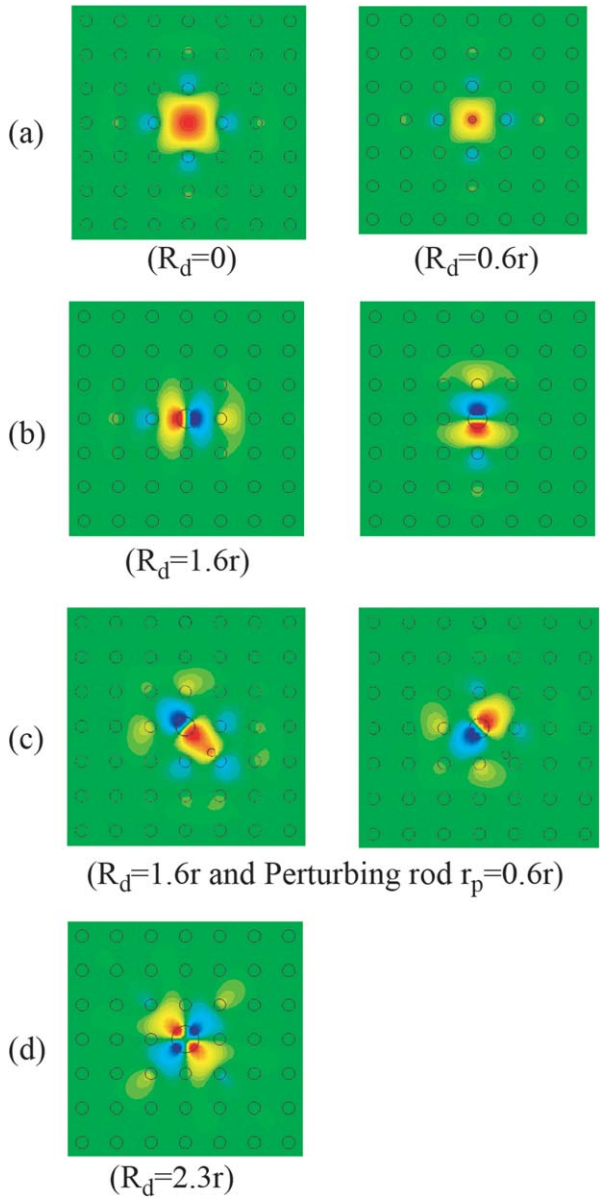

Figure 4 Ez field distribution for four defect modes in the PhC point defect microcavity. (a) Monopole mode (R_d less than r) shown for left $R_d = 0$ and right $R_d = 0.6r$ (b) doubly degenerate dipole mode, $R_d = 1.6r$, (c) coupled dipole mode, and (d) quadrupole mode. [Color figure can be viewed in the online issue, which is available at wileyonlinelibrary.com]

with $N = 3$ shows strong confinement for the TM mode over the frequency range of 1.7–2.3 THz. It should be noted that this single line-defect waveguide is single-moded. Figure 3(d) shows the corresponding dispersion relationship.

3. THE MICROCAVITY AND ITS APPLICATIONS

3.1. Model of the Microcavity and its Resonant Properties

In many emerging THz applications, BPFs play an important role. In particular, the demand for functional, high-performance components such as frequency selective filters is increasing in the field of short-range, high-speed THz communication systems. In this study, we focus our attention on the behavior of the first four resonant modes, that is TM_{110}-, TM_{210}-, TM_{120}-, and TM_{220}-like modes in a point defect microcavity, which are analogous to the resonant modes of a metal square-shaped microwave cavity. These resonant modes are computed by using a supercell approximation.

In the first example, a 2D 7 × 7 supercell containing 49 Si rods in air is considered; see Figure 1(b) with no perturbing rod. The radii of the regular rods are $r = 0.175a$ and the radius of the defect rod, R_d, is $0 < R_d < 2.5r$. The lattice constant, a, is 58.5 μm. The super-cell region is finely meshed, with the number of cells in the x and y dimensions being $N_x = 191$ and $N_y = 191$, respectively. Seven PML layers are used at the boundary of the problem structure to absorb all the outgoing energy. We consider the resonant modes of two types of microcavity coupled to a point-defect. The resonant frequencies and E_z-field distributions of the resonant modes for these cavities are presented in Figure 4. In Figure 4(a), the resonant modes of two microcavities are shown, presented for (left) $R_d = 0$ (a primitive point defect microcavity) and (right) for $R_d = 0.6r$. These modes correspond to the TM_{110}-like monopole modes of a square-shaped microwave cavity, that is, one half sine variation in the x and y directions. In Figure 4(b), $R_d = 1.6r$ which results in the doubly degenerate dipole modes that correspond to the TM_{210} and TM_{120} modes of a square-shaped microwave cavity. For these modes, the field distributions are antisymmetric and the modes disappear into the continuum below the band-gap when the radius of the rod becomes larger than $R_d = 2r$.

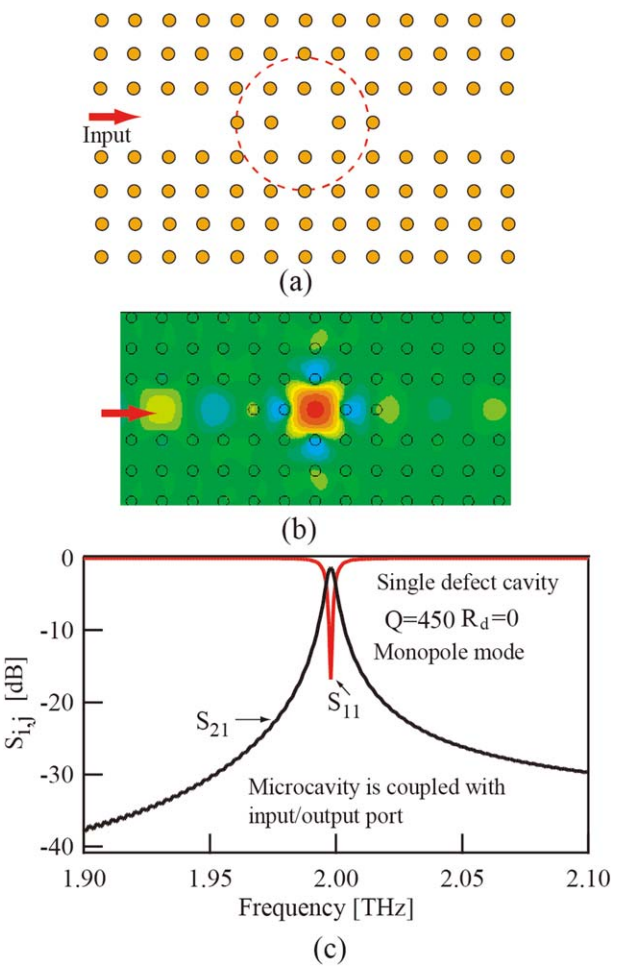

Figure 5 (a) Point defect narrow band microcavity filter without dielectric rod, (b) field distribution for $a = 58.5$ μm and $r = 0.175a$, (c) reflection (red) and transmission (black)characteristics as a function of frequency. [Color figure can be viewed in the online issue, which is available at wileyonlinelibrary.com]

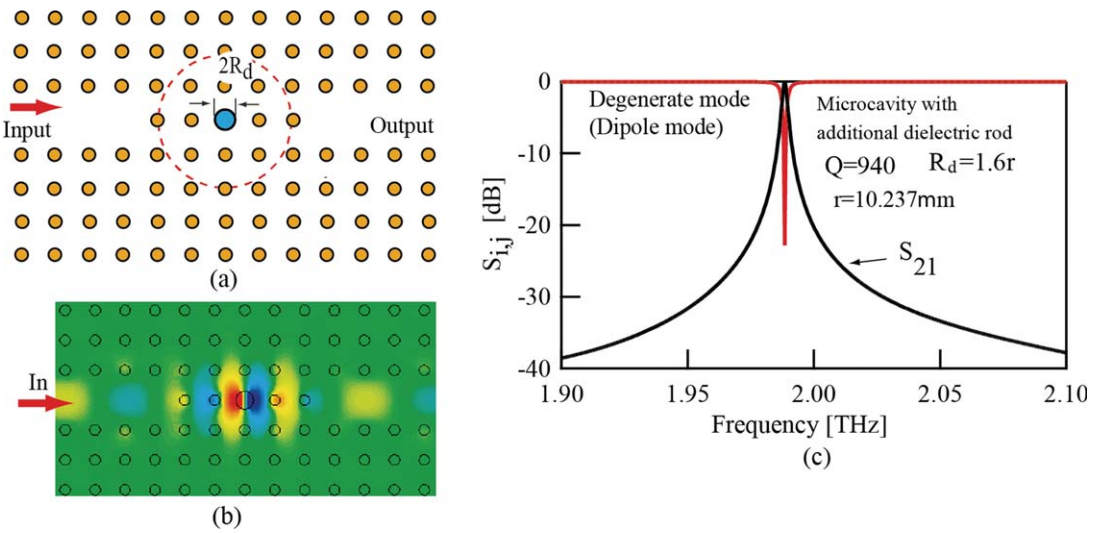

Figure 6 (a) Point defect narrow band microcavity filter with an additional silicon dielectric rod $R_d = 1.6r$, refractive index $n = 3.4$ at its center, (b) field distribution for $a = 58.5$ μm and $r = 0.175a$, and (c) reflection (red) and transmission (black) characteristics as a function of frequency. [Color figure can be viewed in the online issue, which is available at wileyonlinelibrary.com]

A carefully designed PhC cavity can also be used as a high-Q narrowband filter in the THz band. The two degenerated dipole-like modes may exist independently of each other by perturbing the cavity through the introduction of an additional dielectric rod, see Figure 1(b). When no perturbation is present, only a single TM_{210}- or TM_{120}-like mode is excited by the dominant mode of the input/output waveguide. The addition of a small perturbation rod, of radius r_p, causes the degenerate modes

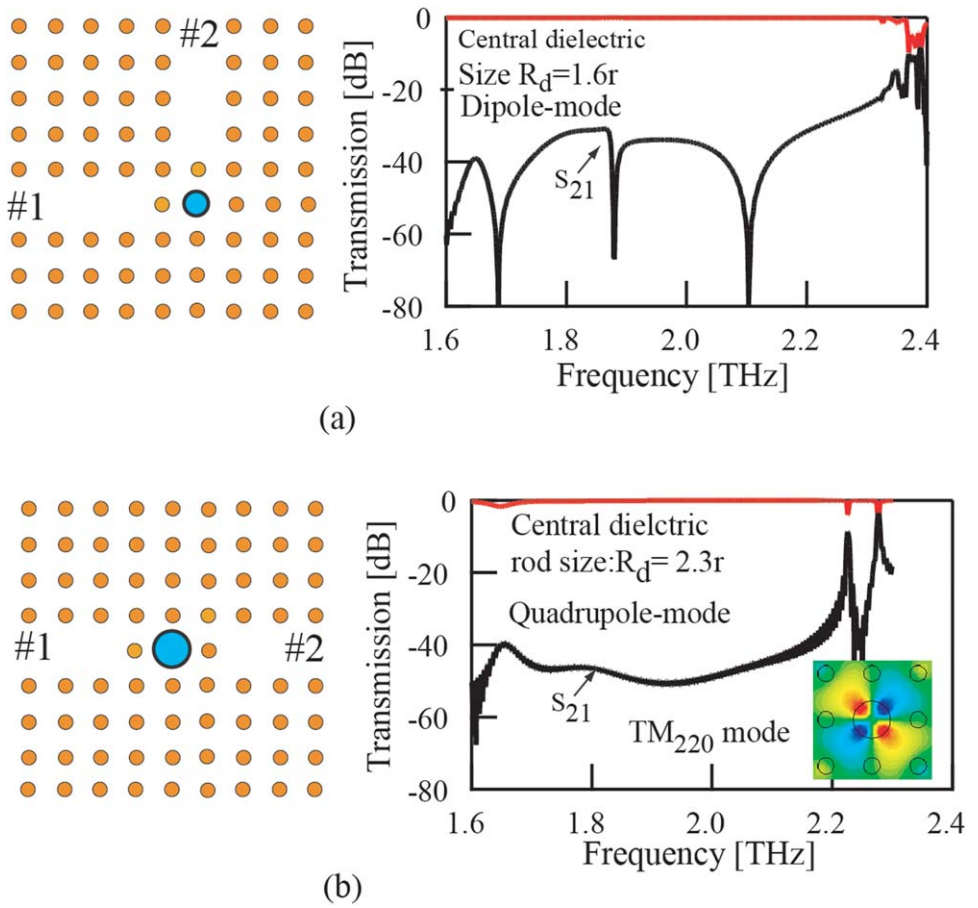

Figure 7 Structure of point defect microcavities with a dielectric rod Rd at their centers, and corresponding reflection (red) and transmission (black) characteristics as a function of frequency. (a) When excited from Port 1, the TM120-like mode is not excited and there is little coupling to the orthogonal Port 2, (b) both Port 1 and Port 2 cannot couple to the quadrupole mode. [Color figure can be viewed in the online issue, which is available at wileyonlinelibrary.com]

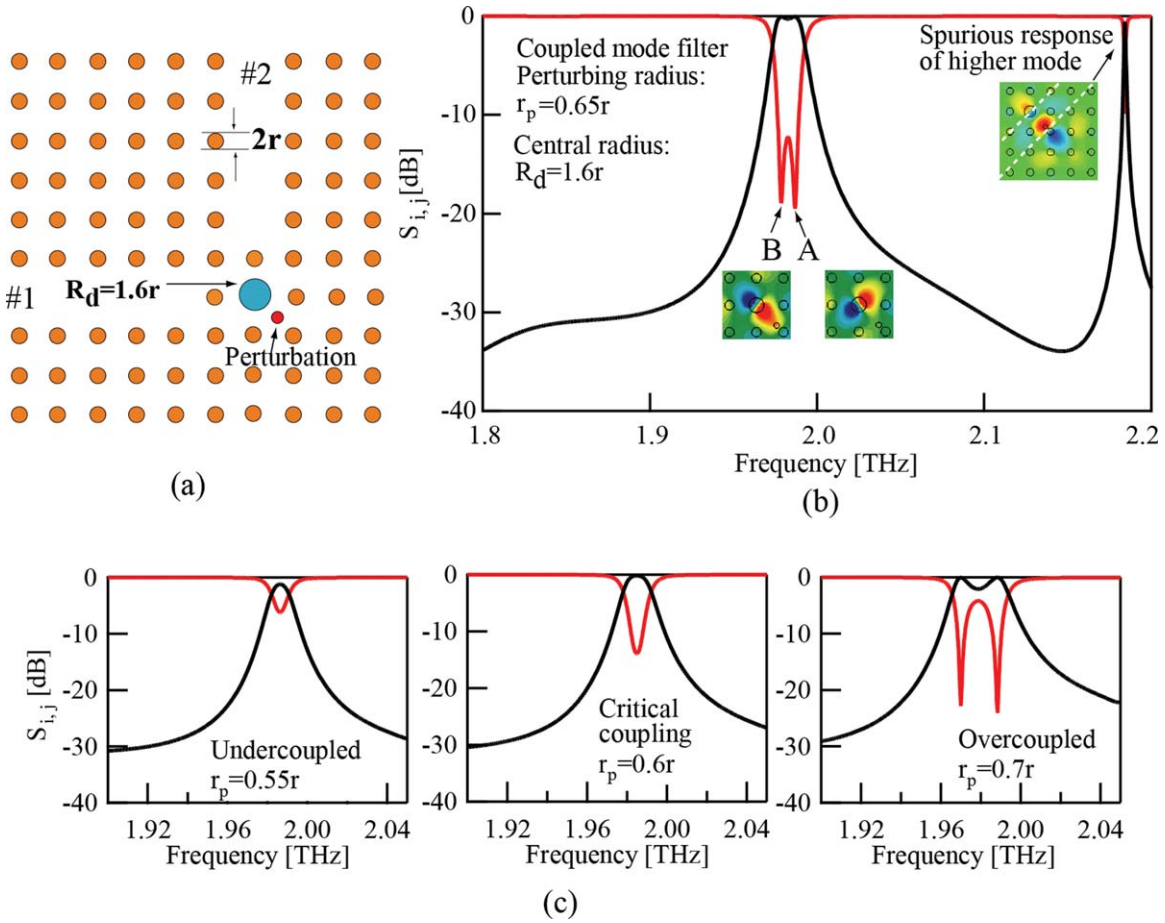

Figure 8 (a) Structure of dual-mode bandpass filter using degenerate modes of photonic crystal point defect cavity showing the placed dielectric rod Rd and small perturbation dielectric rod r_p, (b) transmission (red) and reflection (black) characteristics of dual-mode bandpass filter, (c) double-tuned characteristics of photonic crystal microcavity ($r = 10.2375$ μm, $a = 58.5$ μm, $R_d = 1.6a$, and $n = 3.4$ with, from left to right, undercoupled, critical coupling, and undercoupled conditions. [Color figure can be viewed in the online issue, which is available at wileyonlinelibrary.com]

to split, as shown in Figure 4(c), with the degree of splitting being a function of the radius of the perturbating rod. By increasing the radius R_d of the defect rod, the quadrupole resonant mode (nondegenerate mode) can be excited in the bandgap, Figure 4(d). However, this quadrupole mode does not couple with the fundamental mode of the input/output ports.

Next, we considered the transmission characteristics of two types of microcavities coupled to straight- and right-angled line-defect waveguides. Schematics of the cavities (comprised of square lattices of Si rods in air) along with simulated results are shown in Figures 5–7. For the cavities coupled to straight waveguides shown in Figures 5 and 6, the transmission spectrum peaks at almost 0 dB at frequencies of 2.0 and 1.99 THz, for $R_d = 0$ and $R_d = 1.6r$, respectively. The field patterns in these cases illustrate the high Q nature of the cavities where the field is observed to be strongly confined to a space of $2a$ within the PhC. It is observed that these cavities have a relatively high-Q resonance of at least $Q\sim450$ and $Q\sim940$ for the cases of $R_d = 0$ and $R_d = 1.6r$, respectively. Therefore, the Q of dipole mode, which corresponds to the two degenerate TM_{210} and TM_{120} modes of a metal square-shaped microwave cavity, exceeds that of the fundamental monopole resonant mode. These modes are seen not to couple with the fundamental modes of the input and output ports in the right-angled case shown in Figure 7(a). The quadrupole resonant mode also does not couple with both the input and output ports, as indicated in Figure 7(b).

3.2. Transmission Properties of a Dual-Mode Band-Pass Filter using two Degenerate Modes

In the second example, we again consider a PhC point defect microcavity, $R_d = 1.6r$, but now with the inclusion of a small dielectric perturbation rod of radius r_p, Figure 8(a). With input and output ports in a right-angled configured, both the degenerate modes are excited and coupled to each other due to the addition of this small perturbation rod within the point defect microcavity [9]. The small dielectric perturbation rod, added at a point along a line that is 135° apart from both input and output ports, changes both the field and resonant frequency. This perturbation results in coupling between two orthogonal modes within the microcavity, as shown in Figure 4(c). As a result, a shift in resonant frequency between two orthogonal modes occurs and the two degenerate dipole modes can couple with the dominant mode of input/output ports. The result is a realization of a dual-mode BPF utilizing the doubly degenerate dipole modes of the PhC point defect microcavity. An important issue in the design of this dual-mode filter is the precise control of the mode separation of the two degenerate modes at the working frequency. One approach is to change the radius (R_d) and dielectric constant (ε_s) of the dielectric rod at the center in the cavity, to realize the desired working frequency of the cavity illustrated in Figure 6(a). Two eigenfunctions describe the distribution of the electric field of the TM_{210}- or TM_{120}-like modes; the fields are depicted in Figure 4(c). The distribution of the electric field

in Figure 4(c) can be represented by the sum (= "$TM_{210} + TM_{120}$") and difference (= "$TM_{210} - TM_{120}$") of the modes in Figure 4(b). Figure 8(b) shows the optimized frequency characteristics of the dual-mode filter which is shown to have a stop-band with a rejection region located around 2 THz. The transmission spectra in Figure 8(c) show that the critical coupling is obtained for the perturbing cylindrical radius $r_p = 0.6r$, overcoupled condition occurs for $r_p = 0.7r$, and undercoupled condition for $r_p = 0.55r$. The proposed dual-mode filters have the advantages of a high-unloaded Q, small circuit size, and ease of interfacing with other functional circuits on a PhC platform.

4. CONCLUSION

The applicability of photonic crystal microcavities in the THz regime has been demonstrated through design and simulation. The results presented here indicate a new approach to designing a range of PhC-based devices for filter applications; dual-mode band-pass (or notch) filter, channel drop filter, planar crossing circuits, and so forth. By fine-tuning the lattice arrangement and the radius of the dielectric rods in the neighborhood of the junction or corner discontinuities, a Si/air PhC-based compact dual-mode BPF with a 2–3% rejection bandwidth at around 2.0 THz band has been designed and demonstrated through simulation. A high-Q microcavity has been achieved by modifying conventional point defect cavities through the addition of a dielectric rod in the defect location and the further addition of a perturbing rod into the PhC lattice. It is believed that a new dual-mode PhC point-defect microcavity is a very attractive structure from which to develop compact and high-performance THz band-pass or notch filters on a Si-based single platform.

Future work will extend the time-domain simulations demonstrated here to determine the transmission properties of new PhC planar circuits combining nonradiative dielectric H-guides, together with substrate-integrated waveguides, and PhC in operating in the THz regime.

REFERENCES

1. N. Kukutsu, A. Hirata, T. Kosugi, H. Takahashi, R. Yamaguchi, T. Nagatsuma, and Y. Kado, 10-Gbit/s wireless link systems using the 120-GHz band, In: Tech Dig IEEE AP-S, San Diego, CA, June 2008.
2. R. Mendis and D.M. Mittleman, Comparison of the lowest-order transverse-electric (TE1) and transverse-magnetic (TEM) modes of the parallel-plate waveguide for terahertz pulse applications, Opt Express 17 (2009), 14839–14850.
3. E. Yablonovitch, Inhibited spontaneous emission in solid-state physics and electronics, Phys Rev Lett 58 (1987), 2059–2062.
4. J.D. Joannopoulos, S.G. Johnson, J.N. Winn, and R.D. Meade, Photonic crystals: Molding the flow of light, 2nd ed., Princeton University Press, Princeton, NJ, 2008.
5. K.M. Leung, Plane wave calculation of photonic band structures, In: C.M. Soukoulis (Ed.), Photonic band gaps and localizations, Plenum Press, NY, 1993.
6. CST Microwave Studio Version 5, CST GmbH, Germany, 2004.
7. M. Notomi, K. Yamada, A. Shinya, J. Takahashi, C. Takahashi, and I. Yokohama, Extremely large group-velocity dispersion of line-defect waveguides in photonic crystal slabs, Phys Rev Lett 87 (2001), 1–4.
8. Y. Takakura, H. Nihei, C.P. Chen, and T. Anada, An efficient beam-propagation method for pulse propagation modelling of photonic crystal MMI devices, In: Proceedings of the 39th EuMc, Italy, 2009, pp. 1563–1566.
9. J. Smajic, C. Hafner, and D. Erni, Optimization of photonic crystal structures, J Opt Soc Am A 21 (2004), 2223–2232.

SEAMLESS INTEGRATION OF RZ-DQPSK-DWDM OPTICAL LINKS WITH MISO-OFDM-QPSK SYSTEM FOR FOURTH GENERATION WIDE-AREA COVERAGE MOBILE COMMUNICATION

Yufeng Shao,[1,2] Shikui Wang,[1] Zefu Tan,[1] Yingxiang Luo,[1] and Yushu Lai[1]

[1] College of Electronic and Information Engineering, Chongqing Three Gorges University, Chongqing 404100, China; Corresponding author: syufeng@163.com

[2] School of Electronic and Electrical Engineering, Shanghai Second Polytechnic University, Shanghai 201209, China

Received 2 August 2013

ABSTRACT: *A novel scheme to integrate 10 × 10 Gb/s RZ-DQPSK-DWDM links and MISO-OFDM system is proposed. 106 km optical transmission for RZDQPSK-WDM is implemented, and the balanced demodulation DQPSK signal is transformed into the binary data directly, which is given to MISO-OFDMQPSK system for wireless transmission. Two kinds of MISO-OFDM-QPSK wireless systems are designed: one with two transmitter antennas and one receiver antenna, the other with four transmitter antennas and one receive antenna. The BER performance of almost 10^{-3} is achieved at SNR of 12.5 dB in the system with four transmitter antennas and one receiver antenna, which is better as compared to the other system with two transmitter antennas and one receiver antenna. The results prove that seamless integration of RZ-DPSKDWDM optical links with MIMO-OFDM system is suitable to simultaneously offer higher receiver performance and simplify system configuration for fourth generation wide-area coverage mobile communication.* © 2014 Wiley Periodicals, Inc. Microwave Opt Technol Lett 56:797–801, 2014; View this article online at wileyonlinelibrary.com. DOI 10.1002/mop.28201

Key words: *DWDM; RZDQPSK; multiple-input single-output; OFDM; 4G*

1. INTRODUCTION

From the end of the last century to recent years, the third generation mobile communication system (3G) soon started to be adopted and deployed widely in the world [1, 2]. Today, growing demand for multimedia services including mobile Internet and mobile E-commerce will result in a remarkable increase in 3G wireless networks. The evolution of 3G wireless systems will be followed by the development of 4G wireless systems. In 4G mobile communication systems, more and more types of broadband wireless access services can be introduced to satisfy various users' demand, not only cellular telephone service [3, 4]. Hence, sufficiently high data rate information transmission with high bandwidth efficiency and full seamless integration of wired and wireless links are the important features. For achieving high speed, high capacity, and high quality transmission, the integration of optical fiber communication and wireless communication will play an important role. During the evolution from 3G to 4G, a large number of base stations (BSs) are more possible to be connected with a single central office (CO) for supporting various service types, data rates and end users. In recent years, dense wavelength division multiplexed radio over fiber (DWDM-RoF) systems has been researched and it can resolve the scarcity of available bandwidth [5, 6]. In a DWDM-RoF system, the up conversion and down conversion between the CO and the BSs with micro- or pico-cellular horn antennas are necessary [7, 8], which are very complex and its cost budget is high, as some high-frequency microwave components are